Research Article | Vol. 30, No. 7 / 28 Mar 2022 / Optics Express 11740
Optics EXPRESS

Manipulation of resonance orders and absorbing materials for structural colors in transmission with improved color purity

DONGGYU KIM,[1,3] HYEONWOO KIM,[1,3] INCHEOL JUNG,[1,3] TAE YOUNG KIM,[1] HOJAE KWAK,[1] JONG HOON JUNG,[1] CHANG KWON HWANGBO,[1,4] HUI JOON PARK,[2,5] AND KYU-TAE LEE[1,6]

[1]*Department of Physics, Inha University, Incheon 22212, Republic of Korea*
[2]*Department of Organic and Nano Engineering, Hanyang University, Seoul 04763, Republic of Korea*
[3]*Equal contributors*
[4]*hwangbo@inha.ac.kr*
[5]*huijoon@hanyang.ac.kr*
[6]*ktlee@inha.ac.kr*

Abstract: We present an improved color purity of additive transmissive structural color filters by controlling a resonance order and by inserting a highly absorbing material. The proposed structure consists of a single metal sandwiched by two transparent dielectric media serving as a cavity to minimize the ohmic loss in the metal mirrors, which is distinctly different from a conventional Fabry-Perot (FP) cavity that is in general designed to have two metal mirrors. Low reflections at an air-dielectric interface cause a quality-factor of a resonance to be reduced, causing a degraded color purity, which can be improved by employing a 1st order resonance that exhibits a narrower bandwidth than a fundamental FP resonant mode (0th order). For a red color with the improved purity, introducing an ultrathin absorbing layer in the middle of a top cavity enables the 1st resonance to be trivially influenced while selectively suppressing a 2nd order resonance appearing at the shorter wavelength region. Moreover, angle-insensitive performances up to 60° are attained by utilizing a cavity material with high index of refraction. Besides, the fabrication of the structural coloring devices involves a few deposition steps, thus rendering the approach suitable for applications over the large area. The described concept could be applied to diverse applications, such as colored solar panels, sensors, imaging devices, and decorations.

1. Introduction

Structural colors based on thin-film multilayers, photonic crystals, photonic nanostructures, plasmonic metallic nanocavities, metamaterials, and metasurfaces have generated considerable interest for their potential in achieving improved efficiency, high purity, easy scalability, longstanding stability, and compactness as compared to conventional coloring methods that rely on dyes and pigments [1–24]. Much attention has also been devoted to applying the structural coloring scheme to solar cells to create vivid-colored solar panels [25–30]. Although there have been an increasing number of efforts to create vivid colors in either transmission or reflection from the structures, most of the periodic or aperiodic nanostructures patterned with subwavelength-scale gratings exhibit incident-angle-sensitive properties arising from the momentum matching condition, which needs to be resolved for practical applications [10,12,31–33]. In addition, ohmic losses in a metal cause the efficiency of the transmissive structural colors to be noticeably affected so the structural colors based on surface plasmon polaritons (SPPs) propagating at the metal-dielectric interface and resonances in Fabry-Perot (FP) cavities with two metallic mirrors present the low efficiency still to be addressed.

#453608 https://doi.org/10.1364/OE.453608
Journal © 2022 Received 11 Jan 2022; revised 24 Feb 2022; accepted 5 Mar 2022; published 23 Mar 2022

Optics EXPRESS

Optical cavities have played central roles in a variety of applications, such as bio/chemical sensors, filters, lasers, and optoelectronic devices. Conventional FP cavities generally consist of an optically transparent cavity medium that is separated by two reflecting mirror surfaces, where both a transparency of the cavity and a reflectivity of the mirrors are important to have high quality factor (Q-factor) resulting in a sharp resonance, which is a highly desired property in a number of applications. Highly absorbing media have also been employed as the cavity layer where a non-trivial reflection phase shift at the interface between the absorbing layer and the metal is exploited, thus significantly reducing the thickness of the cavity, despite the resonance with the low Q-factor [7,25,34–40]. Most of the FP cavity designs in previous works have the two metal mirrors that cause light to experience ohmic losses in every round trip in the cavity. Such losses cannot be negligible at a resonant wavelength since light travels multiple times back and forth in the cavity. To minimize the loss occurring in the metal, the simplest design would be to use a single metal mirror yielding a bilayer structure consisting of the cavity medium on the metal. However, the reflection occurring at an interface between air and the cavity is pretty low due to the low refractive index contrast yielding a broad resonance with the low Q-factor, which is not desired for numerous applications. Hence, there is a strong need to develop a cavity design that provides the low ohmic losses in the metal of the FP cavity with a sharp resonance.

In this work, we demonstrate transmissive structural color filters consisting of a single thin metallic mirror between two dielectric media that function as the FP cavity. In dielectric-metal-dielectric filters for blue and green colors, low Q-factor resulting from the low reflection at the interface between air and the cavity is counterbalanced by employing a 1st order resonance whose spectral response is a relatively narrow compared to a fundamental resonance in each FP cavity. Since a 2nd order resonance appears at the short wavelength regime when creating a red color, an ultrathin lossy layer is inserted in the middle of a top FP cavity, which allows the 2nd order resonance to be highly suppressed whereas the 1st order resonance remains with a minor absorption, thus making the resulting color from a magenta to the red. Additionally, the optical response of the structural color filters remains nearly constant in wavelength over a broad range of incidence angles up to 60°, which is attributed to the reduced angle of refraction into the cavity medium with high refractive index. The approach presented in this work could create opportunities for use in various applications, such as image sensors, decorations, and colored see-through solar cells.

2. Results and discussion

Figure 1(a) displays a schematic view of the proposed transmissive structural color filters consisting of two transparent dielectric layers that are separated by a thin metallic mirror. We intend to use a single metal mirror in the proposed structural color filters to mitigate the ohmic losses in the two metal mirrors. A low reflection at the air-dielectric interface leads to a cavity with a low Q-factor yielding a broad spectral profile and hence a poor color purity. Since the 1st order resonance appearing in the shorter wavelength region has a narrow bandwidth as compared to the 0th order resonance (*i.e.*, fundamental mode), the 1st order resonance is exploited to improve a sharpness of a resonant behavior (*i.e.*, high Q-factor) and thus the color purity. Moreover, a dual-cavity configuration comprising cavity #1 – metal – cavity #2, where the 1st order resonant mode is used in each cavity, is adopted to boost the transmission efficiency. Silver (Ag) that presents the highest reflectivity with a trivial absorption at visible wavelengths, titanium dioxide (TiO_2) that has a high index of refraction without the absorption in the visible range, and germanium (Ge) that has a large absorption resulting from a high imaginary part of permittivity at visible frequencies are selected for the mirror, cavity medium, and highly absorbing layer, respectively. The resonance leading to a peak in transmission at a wavelength of λ_m occurs when a net phase shift $\phi_{prop} - (\phi_{r1} + \phi_{r2})$ involving reflection phase changes ϕ_{r1} **and** ϕ_{r2} at the top and bottom interfaces in each cavity, and a round-trip propagation phase change $\phi_{prop}(= 4\pi nL/\lambda_m)$,

Optics EXPRESS

where n and L denote the refractive index and the thickness of the cavity, respectively, is equal to $2m\pi$ (m: integer).

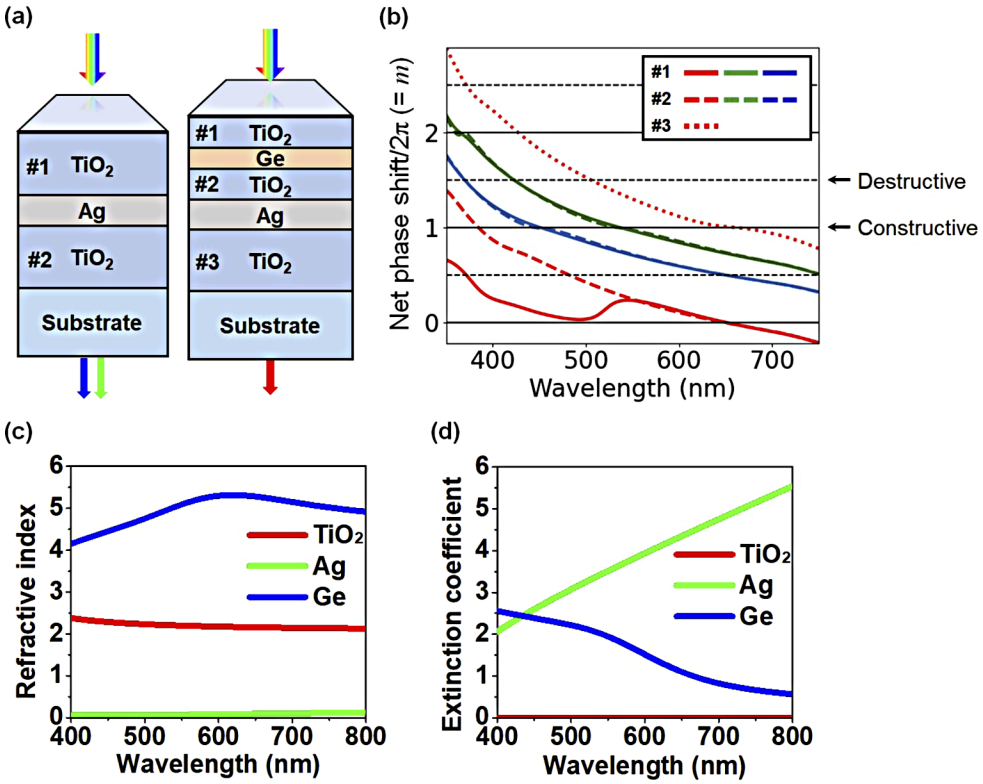

Fig. 1. (a) Schematic diagrams of transmissive structural color filters that exploit a higher-order resonance in dual-cavities consisting of dielectric-metal-dielectric for the blue and green colors. The structure creating the red color involves an ultrathin lossy layer in the middle of the cavity. (b) Net phase shift in the dual cavities for the RGB colors calculated from the proposed structural color filters. (c) Real and (d) imaginary parts of refractive indices of TiO_2, Ag, and Ge, measured by using a spectroscopic ellipsometer (VASE, J. A. Woollam).

Required thicknesses of the cavity for red (R), green (G), and blue (B) colors when employing the 1st order resonance ($m = 1$) can be found by calculating the net phase shift as shown in Fig. 1(b) depicting that the resonance order in the cavities #1 and #2 corresponds to $m = 1$ for the B and G colors where black horizontal solid and dashed lines represent the conditions for constructive and destructive interference, respectively. The y-axis label (*i.e.*, net phase shift/2π) in Fig. 1(b) denotes the order of the resonant mode (*i.e., m*). We note that a top cavity for the R color is divided into two effective cavities with the ultrathin absorbing Ge layer for color generation with the improved purity so the resonance orders in the cavities #1 (red solid line) and #2 (red dashed line) are found to be $m = 0$ while still the resonance order of the cavity #3 (red dotted line) is $m = 1$. The thicknesses of the constituent layers for the RGB color filters are summarized in Table 1.

Such cavity thicknesses can also be found by designing an induced transmission filter of a dielectric – metal – dielectric configuration in order to obtain the highest transmittance for a given metal thickness, where a potential transmittance $\psi_T = \frac{T}{1-R}$ of a metal layer is determined by calculating an optimum exit admittance $Y_{exit,\,opt} = X + iZ$ of the 25 nm-thick Ag layer at

Optics EXPRESS

Table 1. Thicknesses of each layer of the proposed structural color filters

Color	Blue	Green		Red
TiO_2	125 nm	158 nm	TiO_2	65 nm
			Ge	10 nm
			TiO_2	127 nm
Ag	25 nm	25 nm	Ag	25 nm
TiO_2	125 nm	158 nm	TiO_2	203 nm

a target wavelength [41]. Then the thickness of a dielectric matching layer functioning as an antireflection and a narrower-bandwidth coating is found to be $\boldsymbol{d_f} = \frac{\lambda}{2n_f} + \frac{\lambda}{4\pi n_f}\tan^{-1}\left(\frac{2Zn_f}{n_f^2 - X^2 - Z^2}\right)$, where $\boldsymbol{d_f}$ and $\boldsymbol{n_f}$ represent the thickness and the refractive index of the dielectric matching layer, respectively. The induced transmission filters have been applied for highly angle-tolerant filters in the visible spectrum [42,43]. Creating a pure red color requires the 2nd order resonance occurring at 420 nm to be greatly suppressed while preserving the 1st order resonance at 650 nm responsible for the red color generation. This can be achieved by placing an ultrathin absorbing layer in the middle of the cavity to selectively suppress the 2nd order resonance, which will be discussed in more detail later [44–46]. As shown in Figs. 1(c) and (d),wavelength-dependent refractive index (n) and extinction coefficient (k) spectra of TiO_2, Ag, and Ge were measured by using a spectroscopic ellipsometer (VASE, J. A. Woollam), and these values were used in the simulations.

Figure 2(a) reveal the measured and calculated transmittances of the structural color filters at normal incidence, showing that the measured profiles exhibit excellent agreement with the calculated spectra with the difference being that the measured profiles are relatively broad with a lower efficiency. This may be attributed to fabrication defects, non-smooth surfaces, and errors in refractive indices and thicknesses of each layer. When depositing TiO_2 by the e-beam evaporation or the reactive sputtering, an inflow of oxygen is required during the deposition to achieve stoichiometry. The refractive index and the absorption of TiO_2 highly depend on the degree of the oxidation. To achieve the low absorption loss, it is necessary to flow sufficient oxygen during the deposition, which can easily oxidize the thin Ag film by the reactive oxygen gases when depositing TiO_2 on top of the thin Ag film. Although a very thin metal including Ti can function as a good protection layer between the TiO_2 layer and the thin Ag film, the absorption of the metal is significant at visible frequencies, which is not desired for the transmissive structural color applications [47]. From our experience, silicon dioxide (SiO_2) with the thickness of 15 nm is found to be a good protection layer between the TiO_2 layer and the thin Ag film, because SiO_2 is highly transparent at the visible frequencies and can be deposited without the oxygen gases. Note that a 15 nm-thick SiO_2 film was pre-deposited on top of a thin Ag film before depositing TiO_2 as a buffer layer to protect the thin Ag layer. We also note that the thickness of TiO_2 needs to be reduced by about 10 nm with the addition of the 15 nm-thick SiO_2 buffer layer. As can be seen from the figures, the measured transmittances present the 1st FP resonance at 651 nm, 527 nm, and 444 nm with the peak transmittance of 49.18%, 64.63%, and 71.69% for the RGB colors, and the simulated transmission spectra show the resonance at 650 nm, 530 nm, and 450 nm with the peak transmittance of 52.13%, 64.32%, and 74.33% for the RGB colors, respectively. Note that the wavelengths of the 0th, 1st, and 2nd order FP resonances exist at 1275 nm, 450 nm, and 330 nm for the B, 1540 nm, 540 nm, and 359 nm for the G, and 1902nm, 650 nm, and 427 nm for the R, respectively. Figure 2(b) displays optical images of the fabricated RGB color devices with a size of 2.54 cm × 2.54 cm, showing that a background building can be clearly seen through the RGB samples. It is important to note that the only thin-film deposition without complicated lithographic techniques is required for the device fabrication, which can

Optics EXPRESS

be easily expanded on a flexible substrate. In Fig. 2(c), color spaces (x, y) calculated from both measured and simulated transmission spectra described on the CIE 1931 chromaticity diagram to evaluate the purity of the transmissive colors are depicted. The color coordinates (0.399, 0.318), (0.302, 0.442), and (0.206, 0.179) are attained from the experiments (black circles) while (0.452, 0.332), (0.298, 0.448), and (0.194, 0.181) are obtained from the simulations (blue circles) for the RGB colors, respectively. A relatively narrow color gamut is obtained from the experiments, which is ascribed to a relatively broad resonance behavior in the transmission of the fabricated structural color filters as compared to the simulation. The simulated transmission spectra and the color coordinates plotted on the chromaticity diagram are obtained by using a commercial thin-film design software (Essential Macleod), where the measured refractive indices were used. The simulations based on transfer matrix method were performed, where Maxwell's equations and continuity conditions across boundaries between two layers with varied index of refraction are employed to describe electromagnetic waves propagating through a stratified medium. If the electric field of the incident medium is known, the electric field in the last medium can be derived via a simple matrix multiplication. More detailed information regarding the transfer matrix method can be found in the other papers [48,49]. The structural color filters are fabricated by employing the e-beam evaporation on a glass substrate, and the optical properties of the fabricated devices are measured by utilizing a spectrophotometer (Cary 500, Varian).

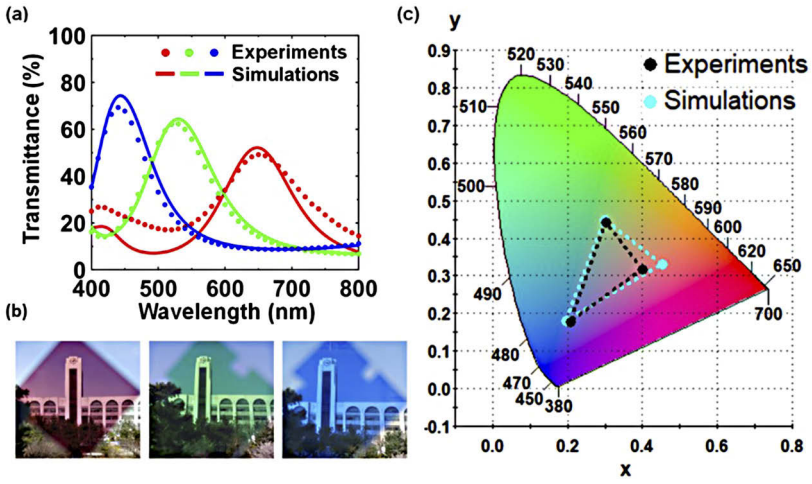

Fig. 2. (a) Measured and simulated spectral curves of transmittance of the proposed structural color filters at normal incidence. (b) Photographs of the structural color filters fabricated on a glass substrate. (c) Color spaces calculated from the measured and simulated transmission spectra, illustrated on the CIE 1931 chromaticity diagram.

We investigate the effect of the order of the FP resonance in the two cavities on the transmission spectra for the RGB colors as provided in Figs. 3(a)–3(c). It has been found that the spectral response gets narrow with a great suppression at off-resonant wavelengths as the order of the resonance increases for all the RGB colors. To evaluate the color purity, Q-factor is calculated from the spectral curves of transmittance shown in Figs. 3(a)–3(c) by $\frac{\lambda_{max}}{FWHM}$, where λ_{max} indicates the wavelength for the transmission peak and the FWHM represents the full width at half maximum. For the structures with $m = 0$ in both top and bottom cavities (cyan colored curves in the transmittance), 1.53, 1.52, and 1.60 of the Q-factor are found, while 4.35, 5.41, and 4.30 of the Q-factor are found for the structures with $m = 1$ in both top and bottom cavities (black colored curves in the transmittance) for the RGB colors, respectively. This shows that the Q-factor of the

Optics EXPRESS

structures with $m = 1$ in the dual-cavities is enhanced by about three times as compared to the structures with $m = 0$.

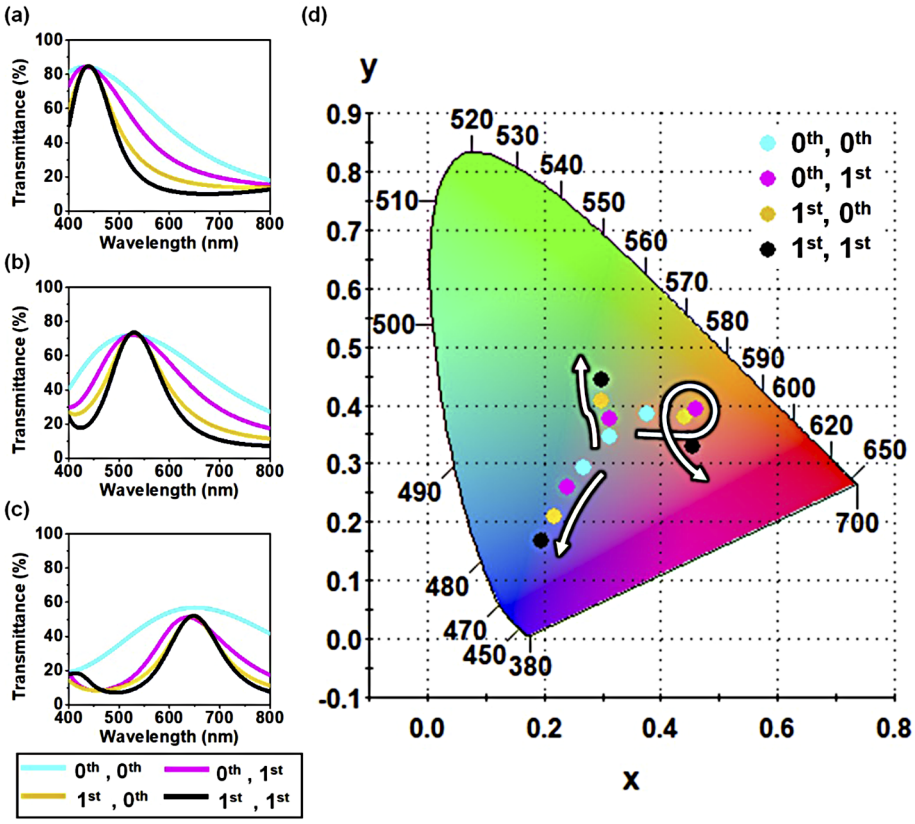

Fig. 3. Effect of a resonance order ($m = 0$ and 1) on the transmission spectra for (a) B, (b) G, and (c) R colors, and (d) the corresponding color spaces on the CIE 1931 chromaticity diagram.

Having the 1st resonance in the two cavities leads to a good filtering capability and thus good color purity as described in Fig. 3(d). It is apparent that the color spaces move toward the exterior of the CIE chromaticity diagram when having the 1st order resonance in the two cavities as compared to the other cases. Note that the further increasing the resonance order in the dual-cavities is found to degrade the color purity because a spacing in wavelength between two successive resonances gets small causing more spectral peaks to appear in the visible region, which are provided in Figs. 4.

Next, the dependence of the Ag thickness on the spectral characteristics is explored. Figures 5(a)–5(c) provide calculated 2D contour plots of the transmittance as a function of the Ag thickness and the wavelength for the RGB colors. With increasing the thickness of the Ag layer, the narrow bandwidth combined with a great elimination of non-resonant wavelength components, which is responsible for the greatly improved color purity, can be achieved with the reduced transmission efficiency that is attributed to the high reflection from the metal mirrors. Figure 5(d) displays that the calculated color spaces of the transmissive structural color filters shift toward the outer part of the chromaticity diagram with increasing the Ag thickness.

In Figs. 6(a) and 6(b), the electric field distributions in the R colored device without the ultrathin lossy layer in the middle of the top FP cavity at $\lambda = 420$ nm and $\lambda = 650$ nm, respectively,

Optics EXPRESS

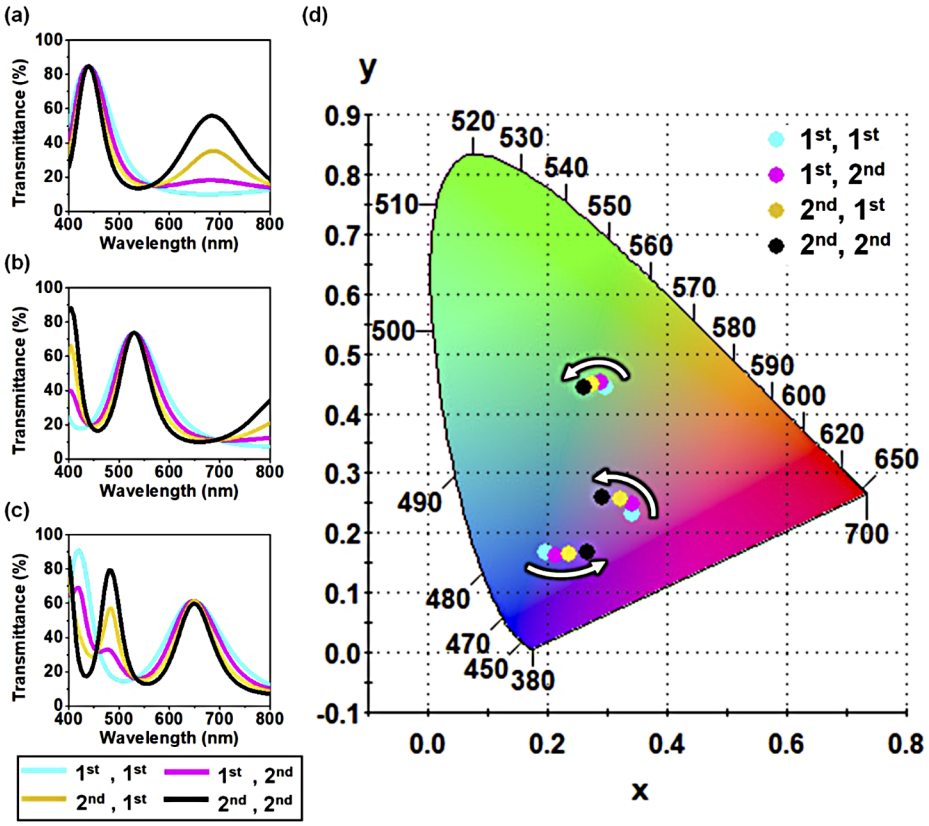

Fig. 4. Influence of the resonance order ($m = 1$ and 2) on the spectral curves of transmittance for (a) B, (b) G, and (c) R color filters, and (d) the corresponding color coordinates described on the CIE 1931 chromaticity diagram.

are provided. Here, the position (x-axis label) represents the depth into the structure where the left-hand side indicates the air incident medium and the right-hand side denotes the substrate. To produce the R color with high purity, it is required to selectively suppress the 2nd order resonance occurring at $\lambda = 420$ nm and the 1st order resonance at $\lambda = 650$ nm, which is responsible for the R color generation, remains without any influence. It can be seen that the field profile in the top cavity at $\lambda = 650$ nm shows the 1st order FP resonance that has a minimum in the middle of the cavity, while the field profile at $\lambda = 420$ nm is the 2nd order FP resonance that has a maximum in the middle of the cavity. This suggests that inserting the highly absorbing material with the ultrathin thickness in the middle of the top cavity results in the great selective suppression of the 2nd order resonance while maintaining the 1st order resonance indicating that the transmission efficiency and the bandwidth of the R color is trivially affected. Ge is chosen as the highly absorbing material as its both real and imaginary parts of refractive index are pretty large at visible frequencies. By placing the 10 nm-thick Ge layer at the center of the top cavity, the significant suppression of the 2nd order resonance at $\lambda = 420$ nm is obtained but the 1st order resonance at $\lambda = 650$ nm is little impacted as can be observed in Figs. 6(c) and 6(d).

The great suppression of the 2nd order resonance at $\lambda = 420$ nm can also be observed in measured and simulated transmission spectra with (red) and without (black) Ge at normal incidence as revealed in Figs. 7(a) and (b). After inserting the ultrathin highly absorbing layer in the top cavity, the effective index of refraction increases so the overall thickness of TiO_2 slightly

Optics EXPRESS

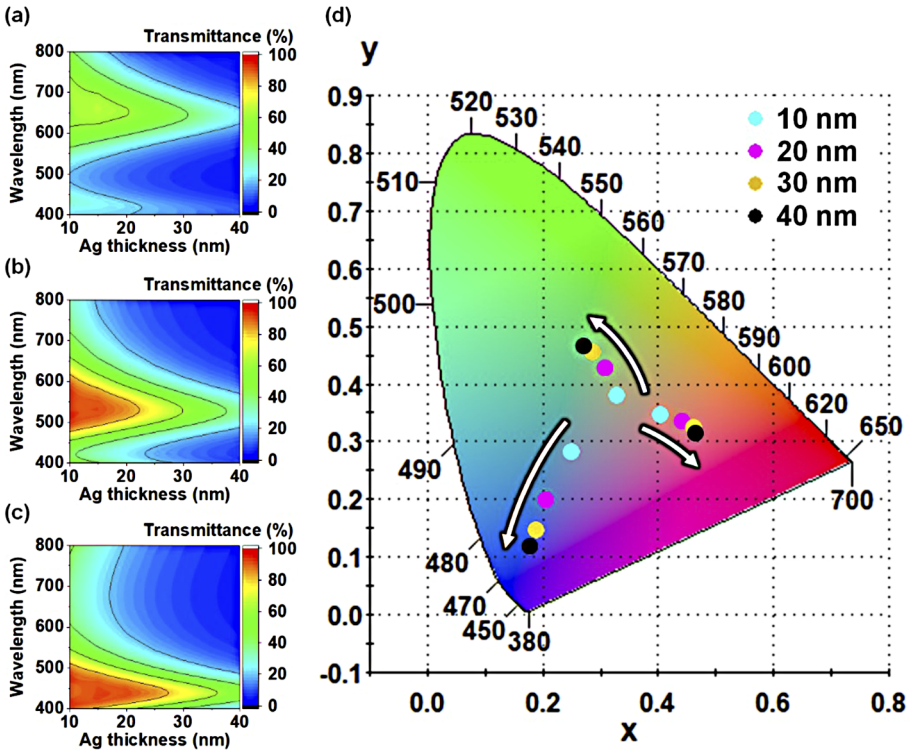

Fig. 5. 2D contour plots of transmittance as a function of the Ag thickness and the wavelength for (a) R, (b) G, (c) B colors, and (d) the corresponding color spaces on the chromaticity diagram.

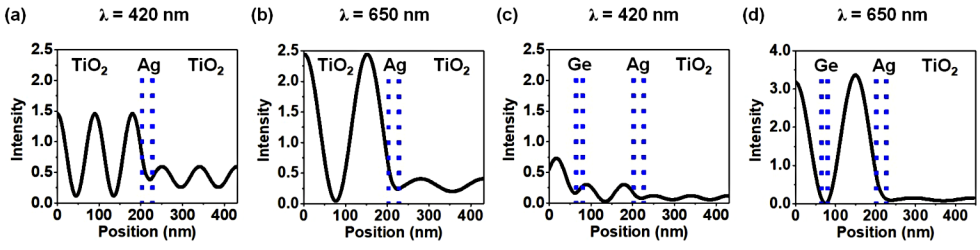

Fig. 6. Normalized electric field intensity distributions of the proposed structural color filters without the ultrathin lossy medium at (a) $\lambda = 420$ nm and (b) $\lambda = 650$ nm, and with the ultrathin absorbing medium at (c) $\lambda = 420$ nm and (d) $\lambda = 650$ nm.

Optics EXPRESS

decreases from 203 nm to 192 nm. The resonance appearing at $\lambda = 420$ nm shown in Figs. 7(a) and 7(b) corresponds to $m = 2$, so the intensity of the electric field for $m = 2$ at the boundary is higher than that for $m = 1$ occurring at $\lambda = 650$ nm. Since the higher resonance order mode is more sensitive with respect to a surface roughness and defects at the boundary, more scattering loss can occur. Errors in refractive indices of TiO_2 and Ag when fitting the measured ellipsometry results with a model can also contribute to the discrepancy. A relatively big discrepancy between the measured and the simulated transmittance at $\lambda = 420$ nm as compared with the discrepancy at $\lambda = 650$ nm may be due to the aforementioned contributions.

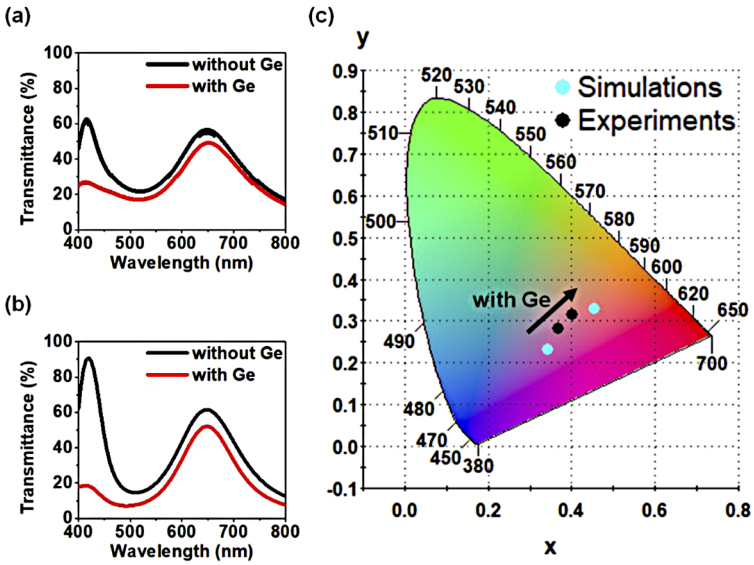

Fig. 7. (a) Measured and (b) simulated transmittances without (black) and with (red) Ge exhibiting that the 2nd order resonance at $\lambda = 420$ nm can be greatly suppressed, while maintaining the 1st order resonance at $\lambda = 650$ nm. (c) Color spaces illustrated on the CIE 1931 chromaticity diagram of the red color device without and with Ge.

Figure 7(c) provides the corresponding color coordinates calculated from both the measured and simulated spectral curves of the transmittance are illustrated on the CIE 1931 chromaticity diagram where the color spaces for the R color device without and with the ultrathin Ge layer in the middle of the top cavity are (0.366, 0.284) and (0.399, 0.318) for the measurements and (0.340, 0.235) and (0.193, 0.171) for the simulations, respectively. This obviously shows the purity of the R color can be improved by introducing the 10 nm-thick Ge layer.

A further suppression of the 2nd order resonance can be accomplished simply by increasing the thickness of the lossy layer although the transmission efficiency at the 1st order resonance for the color generation gets diminished, which is given in Fig. 8. Since the proposed structural color filter is symmetric, inserting the ultrathin lossy layer at the center of the bottom cavity also gives rise to the great suppression as shown in Figs. 8(b) and 8(e). Note that putting the ultrathin highly absorbing medium in the middle of both top and bottom cavities allows the 2nd order resonance to be nearly eliminated leading to the greatly improved color purity but with sacrificing the transmission efficiency as provided in Figs. 8(c) and 8(f).

We also note that Ge at the center of the top cavity can be replaced by any lossy metals including titanium (Ti), nickel (Ni), chromium (Cr), and tungsten (W), which is provided in Fig. 9. As can be seen from the figure, the 2nd order resonance at the shorter wavelength region can be markedly suppressed with Ge as compared to the other lossy materials. The degree of

Optics EXPRESS

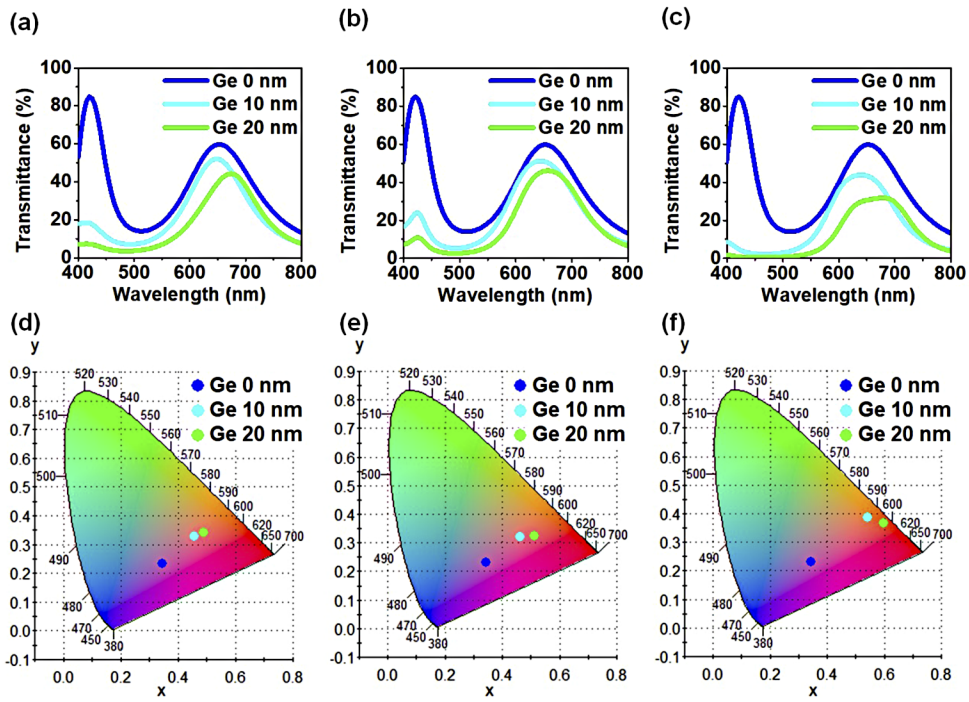

Fig. 8. Simulated transmittances and the corresponding chromaticity diagrams when the light-absorbing layer with the different thickness is inserted in the middle of (a) and (d) the top cavity, (b) and (e) the bottom cavity, and (c) and (f) both top and bottom cavities.

the suppression of the transmittance is dependent on n and k values of the absorbing material and the intensity of the electric field, because the absorption of the material is proportional to the imaginary part of permittivity (ε''), which is $2nk$, of the material ($P_{abs} = \frac{1}{2}\omega\varepsilon''|E|^2$). At $\lambda = 650$ nm for the red color, the absorbing material is inserted at the position where the electric field is almost zero, so the absorption at $\lambda = 650$ nm is nearly negligible regardless of the type of the absorbing material. However, the electric field intensity is high at $\lambda = 420$ nm, so the absorption is highly dependent upon n and k values of the absorbing material. (n, k) at $\lambda = 420$ nm for Ti, Ni, Cr, W, and Ge are (1.61, 2.19), (1.61, 2.48), (2.12, 2.97), (2.99, 2.26), and (4.28, 2.49), respectively. As can be seen from the above n and k values, the product of n and k is the least for Ti and the most for Ge. Thus, the absorption at $\lambda = 420$ nm is the least (most) when using Ti (Ge) for the absorbing medium.

Lastly, we examine how incident angles and polarizations can affect the optical properties of the structural color filters. High refractive index of TiO_2 (2.14 at 550 nm) as the cavity material allows the angle of the refraction into the cavity at oblique angles of incidence to be trivial, thus mitigating the variation in a total phase shift determining the resonant wavelength. Figures 10(a)–10(c) and 10(d) –10(f) depict 2D contour plots of the transmittance as a function of the incident angle and wavelength obtained from the experiments and the simulations, respectively, exhibiting that the measured angle-resolved transmission spectra show good agreement with the simulated spectra. As is seen from the figures, the resonance of the RGB colors remains almost constant for a wide range of incident angles up to 60° under the unpolarized light illumination. It is apparent that a trivial shift of the resonant wavelength and the bandwidth with a minor efficiency drop as increasing the incident angles are observed for all the RGB structural colors.

Optics EXPRESS

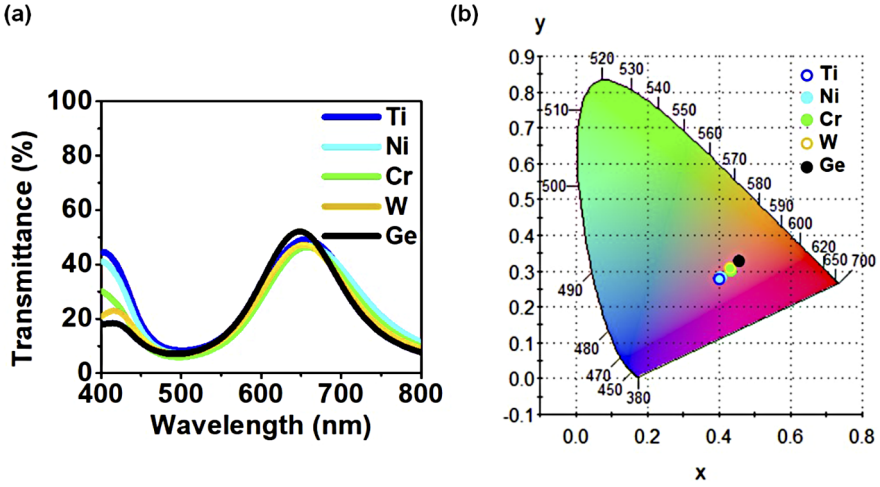

Fig. 9. (a) Simulated transmittance and (b) the corresponding chromaticity diagram of the R color device with various absorbing materials.

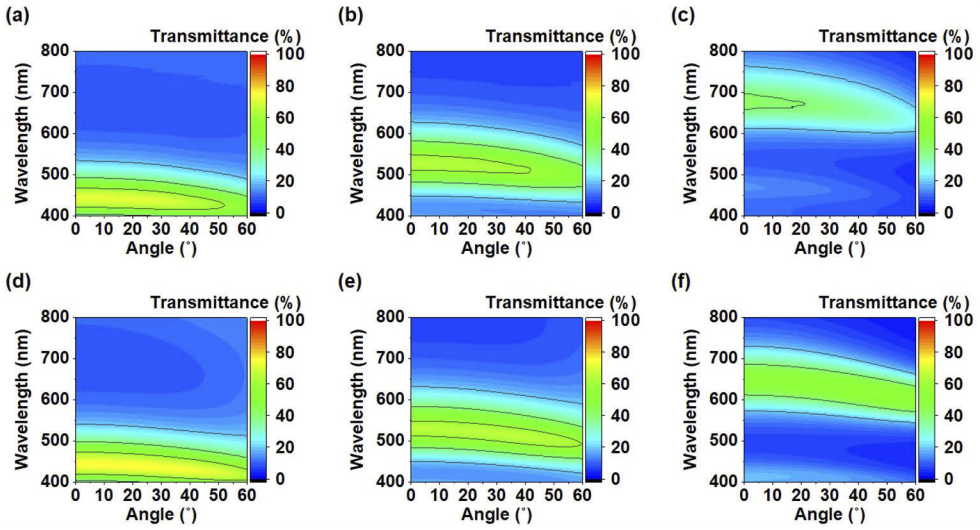

Fig. 10. (a) – (c) Measured and (d) – (f) simulated angle-resolved transmission spectra of the proposed structural color filters under the unpolarized light illumination.

Optics EXPRESS

3. Conclusion

In summary, we have demonstrated the improved color purity of the transmissive structural color filters by manipulating the resonance order in the cavity with the low Q-factor and introducing the highly absorbing material. The broad FP resonance resulting from the low reflection at the air-dielectric interface is compensated by employing the 1st order resonance that shows much narrow spectral characteristics as compared to the fundamental resonance, where the resonant behavior is further enhanced by overlapping the two FP cavities. The 2nd order resonance at the short wavelength region for the R color generation is selectively removed by putting the highly lossy material with the ultrathin thickness in the middle of the top FP cavity, which presents an insignificant effect on the 1st order resonance at the longer wavelength. Furthermore, the high angular tolerant property attributed to the cavity layer with high index of refraction is achieved up to 60° and the large-area samples are readily obtained since the only deposition method is necessary for the device fabrication. The strategy described here could offer an attractive route towards a variety of applications, including decorations, colored solar windows, colorful light-emitting diodes, displays and sensors.

Funding. Ministry of Trade, Industry and Energy (20010035); National Research Foundation of Korea (2019R1F1A1062380, 2020R1A4A1017915).

Disclosures. The authors declare that there are no conflicts of interest related to this article.

Data availability. Experiment and simulation data underlying the results presented in this paper may be obtained from the authors upon reasonable request.

References

1. C. Yang, W. Shen, Y. Zhang, K. Li, X. Fang, X. Zhang, and X. Liu, "Compact Multilayer Film Structure for Angle Insensitive Color Filtering," Sci. Rep. **5**(1), 9285 (2015).
2. C.-S. Park, V. R. Shrestha, S.-S. Lee, E.-S. Kim, and D.-Y. Choi, "Omnidirectional color filters capitalizing on a nano-resonator of Ag-TiO2-Ag integrated with a phase compensating dielectric overlay," Sci. Rep. **5**(1), 8467 (2015).
3. K.-T. Lee, S. Seo, J. Y. Lee, and L. J. Guo, "Strong Resonance Effect in a Lossy Medium-Based Optical Cavity for Angle Robust Spectrum Filters," Adv. Mater. **26**(36), 6324–6328 (2014).
4. Z. Li, S. Butun, and K. Aydin, "Large-Area, Lithography-Free Super Absorbers and Color Filters at Visible Frequencies Using Ultrathin Metallic Films," ACS Photonics **2**(2), 183–188 (2015).
5. C.-S. Park, V. R. Shrestha, S.-S. Lee, and D.-Y. Choi, "Trans-Reflective Color Filters Based on a Phase Compensated Etalon Enabling Adjustable Color Saturation," Sci. Rep. **6**(1), 25496 (2016).
6. K.-T. Lee, S. Seo, J. Yong Lee, and L. Jay Guo, "Ultrathin metal-semiconductor-metal resonator for angle invariant visible band transmission filters," Appl. Phys. Lett. **104**(23), 231112 (2014).
7. M. A. Kats, R. Blanchard, P. Genevet, and F. Capasso, "Nanometre optical coatings based on strong interference effects in highly absorbing media," Nat. Mater. **12**(1), 20–24 (2013).
8. E.-H. Cho, H.-S. Kim, J.-S. Sohn, C.-Y. Moon, N.-C. Park, and Y.-P. Park, "Nanoimprinted photonic crystal color filters for solar-powered reflective displays," Opt. Express **18**(26), 27712–27722 (2010).
9. E.-H. Cho, H.-S. Kim, B.-H. Cheong, P. Oleg, W. Xianyua, J.-S. Sohn, D.-J. Ma, H.-Y. Choi, N.-C. Park, and Y.-P. Park, "Two-dimensional photonic crystal color filter development," Opt. Express **17**(10), 8621–8629 (2009).
10. A. F. Kaplan, T. Xu, and L. J. Guo, "High efficiency resonance-based spectrum filters with tunable transmission bandwidth fabricated using nanoimprint lithography," Appl. Phys. Lett. **99**(14), 143111 (2011).
11. Y.-T. Yoon, H.-S. Lee, S.-S. Lee, S. H. Kim, J.-D. Park, and K.-D. Lee, "Color filter incorporating a subwavelength patterned grating in poly silicon," Opt. Express **16**(4), 2374–2380 (2008).
12. M. J. Uddin and R. Magnusson, "Highly efficient color filter array using resonant Si3N4 gratings," Opt. Express **21**(10), 12495–12506 (2013).
13. V. R. Shrestha, S.-S. Lee, E.-S. Kim, and D.-Y. Choi, "Aluminum Plasmonics Based Highly Transmissive Polarization-Independent Subtractive Color Filters Exploiting a Nanopatch Array," Nano Lett. **14**(11), 6672–6678 (2014).
14. T. Xu, Y.-K. Wu, X. Luo, and L. J. Guo, "Plasmonic nanoresonators for high-resolution colour filtering and spectral imaging," Nat. Commun. **1**(1), 59 (2010).
15. Y.-K. R. Wu, A. E. Hollowell, C. Zhang, and L. J. Guo, "Angle-Insensitive Structural Colours based on Metallic Nanocavities and Coloured Pixels beyond the Diffraction Limit," Sci. Rep. **3**(1), 1194 (2013).
16. S. U. Lee and B.-K. Ju, "Wide-gamut plasmonic color filters using a complementary design method," Sci. Rep. **7**(1), 40649 (2017).
17. F. Cheng, J. Gao, T. S. Luk, and X. Yang, "Structural color printing based on plasmonic metasurfaces of perfect light absorption," Sci. Rep. **5**(1), 11045 (2015).

Optics EXPRESS

18. C. Yang, W. Shen, J. Zhou, X. Fang, D. Zhao, X. Zhang, C. Ji, B. Fang, Y. Zhang, X. Liu, and L. J. Guo, "Angle Robust Reflection/Transmission Plasmonic Filters Using Ultrathin Metal Patch Array," Adv. Opt. Mater. **4**(12), 1981–1986 (2016).
19. W. Yang, S. Xiao, Q. Song, Y. Liu, Y. Wu, S. Wang, J. Yu, J. Han, and D.-P. Tsai, "All-dielectric metasurface for high-performance structural color," Nat. Commun. **11**(1), 1864 (2020).
20. B. Yang, W. Liu, Z. Li, H. Cheng, D.-Y. Choi, S. Chen, and J. Tian, "Ultrahighly Saturated Structural Colors Enhanced by Multipolar-Modulated Metasurfaces," Nano Lett. **19**(7), 4221–4228 (2019).
21. C.-S. Park, I. Koirala, S. Gao, V. R. Shrestha, S.-S. Lee, and D.-Y. Choi, "Structural color filters based on an all-dielectric metasurface exploiting silicon-rich silicon nitride nanodisks," Opt. Express **27**(2), 667–679 (2019).
22. J. Jang, T. Badloe, Y. Yang, T. Lee, J. Mun, and J. Rho, "Spectral Modulation through the Hybridization of Mie-Scatterers and Quasi-Guided Mode Resonances: Realizing Full and Gradients of Structural Color," ACS Nano **14**(11), 15317–15326 (2020).
23. J. Jang, T. Badloe, Y. C. Sim, Y. Yang, J. Mun, T. Lee, Y.-H. Cho, and J. Rho, "Full and gradient structural colouration by lattice amplified gallium nitride Mie-resonators," Nanoscale **12**(41), 21392–21400 (2020).
24. C. Jung, G. Kim, M. Jeong, J. Jang, Z. Dong, T. Badloe, J. K. W. Yang, and J. Rho, "Metasurface-Driven Optically Variable Devices," Chem. Rev. **121**(21), 13013–13050 (2021).
25. K.-T. Lee, J. Y. Lee, S. Seo, and L. Guo, "Colored ultrathin hybrid photovoltaics with high quantum efficiency," Light Sci. Appl. **3**(10), e215 (2014).
26. Y.-M. Sung, M.-Z. Li, D. Luo, Y.-D. Li, S. Biring, Y.-C. Huang, C.-K. Wang, S.-W. Liu, and K.-T. Wong, "A micro-cavity forming electrode with high thermal stability for semi-transparent colorful organic photovoltaics exceeding 13% power conversion efficiency," Nano Energy **80**, 105565 (2021).
27. I. Sajedian, T. Badloe, H. Lee, and J. Rho, "Deep Q-network to produce polarization-independent perfect solar absorbers: a statistical report," Nano Convergence **7**(1), 26 (2020).
28. K.-T. Lee, M. Fukuda, S. Joglekar, and L. J. Guo, "Colored, see-through perovskite solar cells employing an optical cavity," J. Mater. Chem. C **3**(21), 5377–5382 (2015).
29. D.-H. Cho, S.-H. Hong, W.-J. Lee, J. Y. Kim, and Y.-D. Chung, "Colorful solar cells utilizing off-axis light diffraction via transparent nanograting structures," Nano Energy **80**, 105550 (2021).
30. I. Sajedian, H. Lee, and J. Rho, "Design of high transmission color filters for solar cells directed by deep Q-learning," Sol. Energy **195**, 670–676 (2020).
31. M. J. Uddin, T. Khaleque, and R. Magnusson, "Guided-mode resonant polarization-controlled tunable color filters," Opt. Express **22**(10), 12307–12315 (2014).
32. V. Raj Shrestha, S.-S. Lee, E.-S. Kim, and D.-Y. Choi, "Polarization-tuned Dynamic Color Filters Incorporating a Dielectric-loaded Aluminum Nanowire Array," Sci. Rep. **5**(1), 12450 (2015).
33. J. Wang, Q. Fan, S. Zhang, Z. Zhang, H. Zhang, Y. Liang, X. Cao, and T. Xu, "Ultra-thin plasmonic color filters incorporating free-standing resonant membrane waveguides with high transmission efficiency," Appl. Phys. Lett. **110**(3), 031110 (2017).
34. M. A. Kats, D. Sharma, J. Lin, P. Genevet, R. Blanchard, Z. Yang, M. M. Qazilbash, D. N. Basov, S. Ramanathan, and F. Capasso, "Ultra-thin perfect absorber employing a tunable phase change material," Appl. Phys. Lett. **101**(22), 221101 (2012).
35. H. Song, L. Guo, Z. Liu, K. Liu, X. Zeng, D. Ji, N. Zhang, H. Hu, S. Jiang, and Q. Gan, "Nanocavity Enhancement for Ultra-Thin Film Optical Absorber," Adv. Mater. **26**(17), 2737–2743 (2014).
36. V. Steenhoff, M. Theuring, M. Vehse, K. von Maydell, and C. Agert, "Ultrathin Resonant-Cavity-Enhanced Solar Cells with Amorphous Germanium Absorbers," Adv. Opt. Mater. **3**(2), 182–186 (2015).
37. J. Y. Lee, K.-T. Lee, S. Seo, and L. J. Guo, "Decorative power generating panels creating angle insensitive transmissive colors," Sci. Rep. **4**(1), 4192 (2015).
38. H. Song, S. Jiang, D. Ji, X. Zeng, N. Zhang, K. Liu, C. Wang, Y. Xu, and Q. Gan, "Nanocavity absorption enhancement for two-dimensional material monolayer systems," Opt. Express **23**(6), 7120–7130 (2015).
39. Y. J. Yoo, J. H. Lim, G. J. Lee, K.-I. Jang, and Y. M. Song, "Ultra-thin films with highly absorbent porous media fine-tunable for coloration and enhanced color purity," Nanoscale **9**(9), 2986–2991 (2017).
40. M. A. Kats and F. Capasso, "Optical absorbers based on strong interference in ultra-thin films," Laser & Photonics Rev. **10**(5), 735–749 (2016).
41. H. A. Macleod, *Thin-film optical filters / H.A. Macleod* (Hilger, Bristol, 1986).
42. N. Anous, T. Ramadan, M. Abdallah, K. Qaraqe, and D. Khalil, "Planar broad-band and wide-angle hybrid plasmonic IMI filters with induced transmission for visible light applications," Appl. Opt. **56**(31), 8751–8758 (2017).
43. N. Anous, T. Ramadan, M. Abdallah, K. Qaraqe, and D. Khalil, "Planar asymmetric nano-resonators for highly angle tolerant trans-reflective color filters," OSA Continuum **2**(3), 890–904 (2019).
44. K.-T. Lee, S. Y. Han, Z. Li, H. W. Baac, and H. J. Park, "Flexible High-Color-Purity Structural Color Filters Based on a Higher-Order Optical Resonance Suppression," Sci. Rep. **9**(1), 14917 (2019).
45. C. Ji, K.-T. Lee, and L. J. Guo, "High-color-purity, angle-invariant, and bidirectional structural colors based on higher-order resonances," Opt. Lett. **44**(1), 86–89 (2019).
46. D. He, Z. Liu, G. E. Fernandes, T. Shen, D. Oller, D. Pacifici, J. H. Kim, and J. Xu, "High-purity red coloration via mode-selective absorption in a layered thin-film cavity," AIP Adv. **8**(6), 065226 (2018).

Optics EXPRESS

47. L. Jang-Hoon, L. Seung-Hyu, H. C. Kwon, and L. Kwang-Su, "Optical and Structural Properties of TiO_2/Ti/Ag/TiO_2 and TiO_2/ITO/Ag/ITO/TiO_2 Metal-Dielectric Multilayers by RF Magnetron Sputtering for Display Application," J. Korean Phys. Soc. **44**(3), 750–756 (2004).
48. M. C. Troparevsky, A. S. Sabau, A. R. Lupini, and Z. Zhang, "Transfer-matrix formalism for the calculation of optical response in multilayer systems: from coherent to incoherent interference," Opt. Express **18**(24), 24715–24721 (2010).
49. C. C. Katsidis and D. I. Siapkas, "General transfer-matrix method for optical multilayer systems with coherent, partially coherent, and incoherent interference," Appl. Opt. **41**(19), 3978–3987 (2002).